ARCS GRANT
NCC2-452
IN-02
198641
P-26

NASA Technical Memorandum 101075

Documentation of Two- and Three-Dimensional Hypersonic Shock Wave/Turbulent Boundary Layer Interaction Flows

M. I. Kussoy, Eloret Institute, Sunnyvale, California
C. C. Horstman, Ames Research Center, Moffett Field, California

(NASA-TM-101075) DOCUMENTATION OF TWO- AND THREE-DIMENSIONAL HYPERSONIC SHOCK WAVE/TURBULENT BOUNDARY LAYER INTERACTION FLOWS (NASA) 26 p CSCL 01A
N89-20100
Unclas
G3/02 0198641

January 1989

National Aeronautics and
Space Administration

Ames Research Center
Moffett Field, California 94035

SYMBOLS

M	Mach number
p	pressure
P INF	local free-stream static pressure ahead of interaction
PW INF	wall pressure ahead of interaction
q, QW	heat flux
QW INF	heat flux ahead of interaction
r	radial coordinate, distance from model centerline
RHO	density
RHO INF	local free-stream density ahead of interaction
RHOU	mass flux (ρu)
RHOU INF	local free-stream mass flux ahead of interaction
s	distance along model surface measured from flare–cylinder junction
ss	circumferential distance on cylinder measured from fin center line (see fig. 8)
T	temperature
T INF	local free-stream static temperature ahead of interaction
TT	stagnation temperature
TT INF	local free-stream temperature ahead of interaction
u, U	total velocity
U INF	local free-stream velocity ahead of interaction
x	axial coordinate, distance from leading edge of sharp fin (see fig. 8)
y, Y	distance normal to cylinder centerline measured from model surface
δ	boundary-layer thickness
δ^*	compressible displacement thickness,

$$\int_0^{\delta} \left(1 - \frac{\rho u}{\rho_e u_e}\right) \frac{r}{r_w} dy$$

PRECEDING PAGE BLANK NOT FILMED

PAGE 11 INTENTIONALLY BLANK

θ compressible momentum thickness,

$$\int_0^{\delta} \frac{\rho u}{\rho_e u_e}\left(1-\frac{u}{u_e}\right)\frac{r}{r_w}\,dy$$

θ flare, fin, or measurement station angle (see figs. 1 and 8)

ρ density

τ shear stress

Subscripts:

i initial value

0 initial conditions

T wind tunnel stagnation conditions

w wall

∞ local free stream ahead of interaction

DOCUMENTATION OF TWO- AND THREE-DIMENSIONAL HYPERSONIC SHOCK WAVE/TURBULENT BOUNDARY LAYER INTERACTION FLOWS

M. I. Kussoy[1] and C. C. Horstman

Ames Research Center

SUMMARY

Experimental data for a series of two- and three-dimensional shock wave/turbulent boundary layer interaction flows at Mach 7 are presented. Test bodies, composed of simple geometric shapes, were designed to generate flows with varying degrees of pressure gradient, boundary-layer separation, and turning angle. The data include surface-pressure and heat-transfer distributions as well as limited mean-flow-field surveys in both the undisturbed and the interaction regimes. The data are presented in a convenient form for use in validating existing or future computational models of these generic hypersonic flows.

INTRODUCTION

To design realistic aerodynamic vehicles to fly in the hypersonic flow regime, it is of primary importance to be able to predict, with reasonable reliability, the aerodynamic characteristics of such vehicles. Extended and expensive design programs can thereby be significantly improved, and efficient designs identified and studied. Before attempting to predict the aerodynamics of the flow over a complex vehicle (one with a cockpit, fuel tanks, and other appurtenant structures) flying at angle of attack, one should be able to reliably predict basic flow properties, such as surface pressures, heat-transfer distributions, skin friction lines, extent of separation (if any), flow direction, etc., on simple generic shapes. Without the ability to verify computations by experiment on a simple generic body, attempting to predict the flow field over a complex body would be unproductive. The present authors have identified several key features of flows over such vehicles, and have designed test bodies composed of simple geometric shapes over which these flow features can be measured.

The test body employed in the present study consisted of a cone/ogive cylinder at zero angle of attack. Attached to the cylinder were a series of axisymmetric flares or symmetric sharp fins (fig. 1). Both the flare and fin angles were varied, producing shock waves of various strengths, and resulting in both attached and separated flow fields. Detailed boundary-layer surveys have verified a fully developed turbulent boundary layer on the cylinder ahead of the interaction region.

The data obtained during this test program (undisturbed flow-field surveys, surface-pressure and heat-transfer distributions, and several selected flow-field surveys on one flare body) can be used as a data base against which existing computer codes should be verified. In this way, turbulent flow models can be evaluated against flows which are relatively simple (i.e., generic two- and three-dimensional [2-D and 3-D] flows) but exhibit the basic flow characteristics of a more complex flow over a flight vehicle. Presented here are data from the first test series using these test bodies. Additional data obtained include complete flow-field measurements on the flare bodies; these will be presented in a future publication.

---

[1]Eloret Institute.

DESCRIPTION OF EXPERIMENT

Facility

The experiment was conducted in the Ames 3.5-Foot Hypersonic Wind Tunnel where heated, high-pressure air flows through a 1.067-m-diam test section to low-pressure spheres. The nominal free-stream test conditions were total temperature, 900 K; total pressure, 34 atm; free-stream unit Reynolds number, 7×10^6 m^{-1}; and free-stream Mach number, 7.2. The test core diameter was approximately 0.7 m with an axial Mach-number gradient less than 0.12 m^{-1}. Useful test time was 3 min. Run-to-run variations in pressure and Mach number were less than 0.5%. However, the wind-tunnel total temperature varied up to 50 K from run to run, and, in addition, during a single run, it varied about 50 K over the 3-min test time. These variations required special data-reduction procedures which will be discussed later. Free-stream fluctuation measurements have been made in this facility under the above nominal test conditions (ref. 1). The average total temperature and mass-flow fluctuations were 0.83% and 2.7%, respectively.

Test Bodies

Basic test bed. The model consisted of a cone-ogive cylinder, 2 m long and 0.203 m in diameter. It was water-cooled, and surface temperature was maintained at 310 ±5 K during each run. Interchangeable instrumentation ports, 12 cm in diameter and specially contoured to fit flush with the cylinder surface, were placed at 25-cm intervals along the cylinder in a single line and at 50-cm intervals in another single line 180° away. Individual ports were instrumented with static pressure taps and thermocouples. One port accommodated a survey mechanism to which static pressure, total pressure, and total temperature probes could be attached for flow-field surveys. Additional static pressure taps and thermocouples were located at 5-cm intervals along the entire length, in a single line 90° away from the instrumentation ports. At several points along the cylinder, static pressure taps were located every 90° around it.

Flares. Four flares were tested, with half angles of 20°, 30°, 32.5°, and 35°. They were placed on the cylinder 139 cm from the cone tip, as shown in figure 1(a). The flares were fabricated in two halves. A 2.5-cm-wide slit was milled in one of the halves, along its axis. Contoured plates 0.254 cm thick, either blank or instrumented, covered the slit. Instrumentation on an individual flare could thus be easily changed between tunnel runs. For the flow survey runs, the flare was positioned over the port containing the survey mechanism (see below) at the desired streamwise location, and a small access hole was drilled through the contoured cover plate. This access hole accommodated the particular survey probe being used.

Fins. Three noninstrumented fins, with half angles of 10°, 15°, and 20°, were investigated. They were bolted to the cylinder 120 cm from the tip, as shown in figure 1(b).

Instrumentation

Surface pressure. Static pressure taps of 0.16-cm internal diameter were located along the model surface as well as in several instrumentation ports, and were connected with short lengths of stainless steel tubing (10 to 15 cm long) to strain-gauge, absolute-pressure transducers. In situ calibrations were made by varying the wind tunnel test-section pressure, and recording it using a Datametric strain gauge differential pressure cell which had been calibrated previously with a dead-weight tester. All calibrations were linear, and were repeatable to within 1%. In addition, a pressure-scanning system was used to obtain accurate measurements of the low static pressures present on the model surface and in the flow field. This system was designed to be calibrated in situ with carefully monitored pressures. Before each run, a

transducer reading was obtained at the wind tunnel starting pressure (approximately 0.01 atm) to determine the zero offset of the gauges. The transducers were water-cooled, and all were located within the model.

Surface heat transfer. Surface heat transfer was measured by the transient thin-skin technique. For measurements on the cylinder surface, ports were instrumented with chromel-alumel thermocouples spotwelded to the interior surface, approximately 1 cm apart. These instrumented ports were used to measure the heat transfer upstream of the flare bodies and also on the surface adjacent to the fin. (In addition, four Schmidt-Boulter heat-transfer gauges were placed in the port upstream of the flares.) Heat transfer was also measured along a ray of each flare surface by instrumenting a contour plate with chromel-alumel thermocouples spaced 0.5, 1, or 2 cm apart. For these tests, the entire model was kept at room temperature, then inserted into the flow after the desired flow conditions were obtained. Depending on the thermocouple location, the temperature rise (with the internal model water-cooling system disconnected) varied from 10 to 50 K during a typical 30-sec heat-transfer run. The data were reduced by obtaining a least squares linear fit of $\ln [(T_T - T_W)/(T_T - T_{Wi})]$ versus time. The variation of the wind tunnel total temperature (T_T) with time was included. Calculations using the procedures outlined in reference 2 indicated that for the above test conditions the temperature of the interior wall rises to that of the exterior wall after 2 sec, and that longitudinal conduction errors are less than 5% of the measured convective heat transfer. Therefore no corrections were applied to the data.

Survey mechanism. Flow-field surveys were obtained with the survey mechanism shown in figure 2. A precision power screw was driven by a stepping motor, whose shaft was capable of turning in controlled increments as small as 1.8°, or in any multiple of 1.8°. The vertical resolution of this mechanism was 0.0003 cm. The rotary motion of the motor shaft was coupled to the precision screw with antibacklash bevel gears, and the vertical position was obtained from a three-turn precision potentiometer driven by an antibacklash worm gear.

Pitot pressure probe. Pitot pressures in the flow field were measured by a stainless steel probe, as shown in figure 3. The probe was calibrated in a free-jet facility, matching Mach number, velocity, and density with the present test conditions. This calibration indicated that the error due to rarefaction effects was less than 1%; therefore no corrections were applied to the pitot data. The probe was attached to a water-cooled pressure transducer located within the model, connected with a short length (about 8 cm) of stainless steel tubing. The pressure-transducer calibration procedure was identical to the surface-pressure procedure discussed previously.

Static pressure probe. Static pressures in the flow field were measured by another stainless steel probe, as shown in figure 4. This probe is geometrically similar to one used by Behrens (ref. 3), i.e., a 10° cone-cylinder. Independent calibrations to account for viscous interaction effects agreed with Behrens' calibration. The maximum viscous corrections applied to the data were 2% in the interaction region and 7% in the undisturbed region ahead of the shock wave. The probe was attached, by a short length (about 8 cm) of stainless steel tubing, to a water-cooled pressure transducer located within the model. The pressure-transducer calibration procedure was identical to the surface-pressure procedure discussed previously.

Total temperature probe. Total temperatures in the flow field were measured with the probe shown in figure 5. This probe was designed using a concept suggested by Vas (ref. 4). An unshielded, butt-welded chromel-alumel thermocouple (0.3 cm long by 0.007 cm thick) was supported by tapered chromel and alumel posts. A second chromel-alumel thermocouple was formed at the end of the alumel support (fig. 5). This allowed a simultaneous measurement of the butt-welded thermocouple junction and the probe support.

Corrections for radiation, conduction, and recovery factor were made following the method described in reference 4. To make these corrections, one must know the local Mach number and Reynolds number; this requires an iterative procedure using the pitot and static pressure data. In the present study,

radiation effects were negligible. Independent calibrations of these probes in the wind tunnel free stream indicated a maximum total temperature error of 1.5%.

Test procedure. Data were obtained during a series of runs with the wind tunnel operating at the nominal conditions described above. Before each run, the test body was positioned outside the open jet. Flow was then initiated. When the desired test conditions were reached, the model was inserted into the test stream. The model was retracted before tunnel shutdown.

To establish the presence of a fully developed, equilibrium, hypersonic, turbulent boundary layer approaching the interaction region, pitot pressure, static pressure, and total temperature surveys of the boundary layer were taken at a distance of 133 cm from the model nose. For these undisturbed boundary-layer surveys, the cone-ogive-cylinder test body was run devoid of any flare or fin appendages. Previous tests using this identical cone-ogive-cylinder test body (see ref. 5) established the existence of a fully developed, self-similar turbulent boundary layer with a negligible pressure gradient 100 to 300 cm from the model tip. Natural transition from laminar to turbulent flow occurred between 40 and 80 cm from the model tip. Velocity, density, and pressure profiles were obtained from the pitot and static pressure and total temperature surveys. Each survey was taken during a single test run. In traversing the flow field, the probe was stopped at each location for a few seconds to ensure that there was no time lag in the pressure or temperature measurement. Survey data were obtained up to 3.0 cm from the (cylindrical) model surface. The static pressure at the model surface was monitored continuously during all traverses to verify that the data were free from interference effects.

Axisymmetry. Surface pressure was measured at selected axial positions at 90° intervals around the model. Variations in these measurements were less than could be accounted for by the experimental error in measurement. Also, results from surface-oil-film studies obtained while investigating the higher-angled flare bodies showed symmetric separation lines around the model. From these results it was concluded that the flow was axisymmetric.

EXPERIMENTAL RESULTS

Local Free-Stream Conditions

Surveys of pitot and static pressure and total temperature were obtained at a location upstream of the interaction region (133 cm downstream from the tip) to determine the undisturbed local free-stream conditions immediately ahead of the flow field under investigation. The velocity profiles obtained from these mean flow-field surveys were transformed using the Van Dreist II transformation (ref. 6) into incompressible coordinates, and are shown in figure 6 in law-of-the-wall coordinates. Also shown on this plot is Coles' universal law of the wall (ref. 7). These profiles verify the presence of a hypersonic, fully developed turbulent boundary layer immediately upstream of the interaction region for the axisymmetric flared test bodies. By using the law-of-the-wall concept, surface skin friction was determined; this value was $C_f = 1.22 \times 10^{-3}$. For any turbulent-model-verification procedure, these initial boundary-layer conditions should be verified (or set) by the computation. The measured local free-stream conditions are given in table I. For the 3-D sharp-fin flows, the fin leading edge is slightly ahead of this station (13 cm). Therefore, a suitable boundary-layer code should be used to extrapolate upstream for appropriate initial conditions.

Flow-field surveys were taken on the unadorned cylindrical test body to determine the initial boundary-layer conditions as described above. These surveys were taken at a location 133 cm from the tip, and up to $y = 3$ cm. Surveys were also taken at three positions, $s = 5.5$, 10.3, and 15.5 cm, along a ray on the 20° flare (s is measured along the flare surface). Quantities measured during these surveys, as well as derived quantities, are presented in table II for the undisturbed boundary layer and in table III for

the flow field over the 20° flare. The shock wave produced by the flare is evident in the data for the two forward surveys. The shock wave was not reached at the most rearward station. (A complete set of surveys has been planned for all the flares. Survey results will be presented in a future publication.)

Surface Measurements

The surface-pressure distribution 50 cm upstream of the flare-placement position is shown in figure 7. It is evident that the resulting pressure gradient, 10%/m, is small enough that we may consider negligible any effect of small longitudinal displacement of the $s = 0$ point of the flare and fin bodies away from this nominal position for this investigation.

Surface-pressure and heat-transfer distributions over the four flares are given in table IV. The separation locations as measured by the oil-flow visualization technique were $s = 0$ for $\theta = 20°$ and 30°, $s = -3.1$ cm for $\theta = 32.5°$, and $s = -6.3$ cm for $\theta = 35°$. Reattachment locations could not be determined. For the surface conditions on the cylinder–flare combination, s represents the distance along the cylinder upstream of the $s = 0$ point (the negative values in table IV), and then the distance along a ray of the flare (the positive values). For the flares, the $s = 0$ point was at a distance of 139 cm from the model tip. For the sharp-fin flows, the fin leading edge was placed 120 cm from the model tip. The surface measurements adjacent to the fin were taken using an instrumented port on which pressure taps and thermocouples were placed in two concentric arcs, as shown in figure 8. (The definitions of x, ss, and θ are also shown in this figure.) The positions of the pressure taps and thermocouples on the port are given in table V. The surface data for the cylinder–fin combination is given in table VI. Surface oil-flow data were also obtained for the sharp-fin flows. For all the fin angles, both a primary and a secondary convergence line were observed. The primary separation line for all cases was located approximately where $p_w/p_{w\ inf} = 1.2$. The secondary separation line was near the fin, approximately one-third of the distance between the fin and the primary separation line. Unfortunately these results would not show up well enough in black and white for photographs to be included in this report.

These data are average values obtained from many runs. (Thermocouple and Schmidt-Boulter gauge data were averaged to obtain heat-transfer distributions upstream of the flares.) The surface heat-transfer results were not corrected for the small longitudinal conduction errors (less than 5%) but were corrected for run-to-run variations in wind tunnel temperature. This was done by assuming that the heat flux divided by the driving potential $(T_{Ti} - T_{Wi})$ is invariant for small changes in total temperature. Therefore: $q_{corrected} = q_{measured}\,[(T_{Ti} - T_{Wi})_{nominal}/(T_{Ti} - T_{Wi})_{measured}]$.

Experimental Uncertainties

The uncertainties in the surface-pressure and heat-flux measurements were estimated to be ±10%. For the flow-field quantities, the estimated uncertainties are ±1.5% for the total temperature, ±10% for the static pressure, ±6% for the static temperature, ±12% for the density, and ±3% for the velocity. The uncertainty in y is ±0.02 cm. These uncertainties in the flow-field variables are due principally to zero offsets in the pressure measurements. Since each survey was obtained with a single probe, the uncertainty of the vertical variation in these flow-field quantities is significantly less than the numbers quoted above.

CONCLUDING REMARKS

Several cases of shock wave/hypersonic turbulent boundary layer interaction flows over a cone-ogive cylinder with attached flares and fins have been experimentally investigated. The resulting flows

were axisymmetric (with and without separation) and 3-D (with separation). These particular flows were chosen because they were relatively simple, but exhibited the same basic characteristics as complex hypersonic vehicles do.

Surface-pressure and heat-transfer distributions, as well as results of several flow-field surveys (in both the undisturbed and the interaction regimes) are presented here. These data will be useful for validating present or future turbulence models. This validation procedure is necessary before attempts are made to compute more complex flows over actual flight vehicles.

REFERENCES

1. Owen, F. K.; Horstman, C. C.; Stainback, P. C.; and Wagner, R. D.: Comparison of Transition and Freestream Disturbance Measurements Obtained in Two Wind Tunnel Facilities. AIAA Paper 74-131, Jan. 1974.

2. George, A. R.; and Reinecke, W. G.: Conduction in Thin-Skinned Heat Transfer and Recovery Temperature Models. AIAA J., vol. 1, no. 8, Aug. 1963, pp. 1956-1958.

3. Behrens, W.: Viscous Interaction Effects on a Static Pressure Probe at M = 6. AIAA J., vol. 1, no. 12, Dec. 1963, pp. 2864-2866.

4. Vas, I. E.: Flow Field Measurements Using a Total Temperature Probe at Hypersonic Speeds. AIAA J., vol. 10, no. 3, March 1972, pp. 317-323.

5. Horstman, C. C.; and Owen, F. K.: Turbulent Properties of a Compressible Boundary Layer. AIAA J., vol. 10, no. 11, Nov. 1972, pp. 1418-1424.

6. Van Driest, E. R.: The Problems of Aerodynamic Heating. Aerospace Eng. Rev., vol. 15, 1956, pp. 26-41.

7. Coles, D. E.: The Turbulent Boundary Layer in a Compressible Fluid. Rand Corp., Report R-403-PR, 1962.

TABLE I.– LOCAL FREE-STREAM CONDITIONS

$M_\infty = 7.05$

$T_\infty = 81.2$ K

$p_\infty = 576$ N/m^2

$\rho_\infty = 0.0252$ kg/m^3

$T_w = 311$ K

$U_\infty = 1274$ m/sec

$\delta o = 2.5$ cm

$\delta_o^* = 0.74$ cm

$\theta_o = 0.065$ cm

$\tau_{w_\infty} = 25$ N/m^2

$q_{w_\infty} = 9300$ W/m^2

$Re_{\delta_o} = 1.45\times10^5$

$Re_{\theta_o} = 3.8\times10^3$

$Re/m = 5.8\times10^6$

$$C_{f_\infty} = \frac{\tau_{w_\infty}}{1/2\ \rho_\infty U_\infty^2} = 1.22\times10^{-3}$$

$$C_{h_\infty} = \frac{q_{w_\infty}}{\rho_\infty U_\infty C_p(0.9T_T - T_w)} = 0.59\times10^{-3}$$

TABLE II.– FLOW FIELD SURVEY

UPSTREAM BOUNDARY LAYER

Y(CM)	M	P / P INF	RHO / RHO INF	T / T INF	U / U INF	RHOU / RHOU INF	TT / TT INF
0.000	0.000	1.000	0.269	3.711	0.000	0.000	0.350
0.065	1.547	1.000	0.217	4.600	0.470	0.102	0.638
0.093	2.177	1.000	0.264	3.793	0.601	0.159	0.690
0.120	2.745	1.000	0.310	3.223	0.699	0.217	0.752
0.180	3.111	1.000	0.338	2.959	0.759	0.257	0.805
0.250	3.356	1.000	0.362	2.760	0.791	0.287	0.830
0.320	3.610	1.000	0.388	2.576	0.822	0.319	0.858
0.390	3.835	1.000	0.424	2.359	0.836	0.354	0.858
0.460	4.070	1.000	0.454	2.204	0.858	0.389	0.877
0.620	4.626	1.000	0.537	1.862	0.896	0.481	0.905
0.770	5.248	1.000	0.643	1.555	0.929	0.597	0.930
0.940	5.739	1.000	0.730	1.371	0.954	0.696	0.954
1.090	6.070	1.000	0.794	1.260	0.967	0.767	0.966
1.260	6.340	1.000	0.839	1.192	0.982	0.824	0.986
1.450	6.599	1.000	0.901	1.110	0.986	0.889	0.986
1.640	6.820	1.000	0.951	1.051	0.992	0.944	0.991
1.900	6.962	1.000	0.978	1.023	0.999	0.977	1.000
2.150	7.022	1.000	0.993	1.007	1.000	0.993	1.000
2.400	7.048	1.000	1.000	1.000	1.000	1.000	1.000
2.700	7.050	1.000	1.000	1.000	1.000	1.000	1.000
3.000	7.050	1.000	1.000	1.000	1.000	1.000	1.000

TABLE III(a).– FLOW FIELD SURVEYS

20 DEGREE FLARE – S = 5.5 CM

Y(CM)	M	P / P INF	RHO / RHO INF	T / T INF	U / U INF	RHOU / RHOU INF	TT / TT INF
0.000	0.000	10.539	2.840	3.711	0.000	0.000	0.350
0.053	2.768	10.539	2.793	3.774	0.763	2.130	0.881
0.096	2.800	10.539	2.745	3.840	0.778	2.136	0.907
0.145	2.878	10.539	2.762	3.815	0.797	2.203	0.931
0.195	2.983	10.539	2.865	3.679	0.812	2.326	0.939
0.290	3.266	10.539	3.126	3.372	0.851	2.660	0.968
0.395	3.701	10.120	3.488	2.901	0.895	3.120	0.992
0.495	3.980	9.760	3.728	2.618	0.914	3.406	0.998
0.590	4.043	9.461	3.692	2.562	0.918	3.391	1.000
0.790	7.050	1.000	0.994	1.006	1.004	0.997	1.006
0.990	7.050	1.000	0.994	1.006	1.004	0.997	1.006
1.175	7.050	1.000	0.996	1.004	1.003	0.998	1.004
1.360	7.050	1.000	0.996	1.004	1.003	0.998	1.004

TABLE III(b).– FLOW FIELD SURVEYS

20 DEGREE FLARE – S = 10.3 CM

Y(CM)	M	P / P INF	RHO / RHO INF	T / T INF	U / U INF	RHOU / RHOU INF	TT / TT INF
0.000	0.000	11.976	3.227	3.711	0.000	0.000	0.350
0.055	2.250	11.976	2.358	5.079	0.718	1.693	0.938
0.100	2.859	11.976	3.031	3.951	0.806	2.443	0.955
0.140	3.107	11.976	3.340	3.585	0.835	2.788	0.963
0.185	3.157	11.976	3.404	3.519	0.840	2.859	0.965
0.270	3.253	11.976	3.485	3.437	0.856	2.982	0.980
0.360	3.336	11.976	3.584	3.341	0.865	3.101	0.986
0.450	3.417	11.976	3.673	3.260	0.875	3.216	0.994
0.650	3.605	11.976	3.939	3.040	0.892	3.513	1.000
0.850	3.763	11.976	4.196	2.854	0.902	3.785	1.000
1.050	3.835	11.976	4.335	2.763	0.904	3.921	0.995
1.200	4.089	9.581	3.848	2.490	0.916	3.524	0.989
1.420	7.052	1.000	1.002	0.998	1.001	1.003	1.001
1.620	7.052	1.000	1.002	0.998	1.001	1.003	1.001

TABLE III(c).– FLOW FIELD SURVEYS

20 DEGREE FLARE – S = 15.5 CM

Y(CM)	M	P / P INF	RHO / RHO INF	T / T INF	U / U INF	RHOU / RHOU INF	TT / TT INF
0.000	0.000	12.335	3.324	3.711	0.000	0.000	0.350
0.065	2.533	12.335	2.948	4.185	0.735	2.166	0.881
0.083	2.747	12.335	3.143	3.925	0.772	2.426	0.906
0.100	2.997	12.335	3.395	3.633	0.810	2.752	0.933
0.138	3.121	12.335	3.495	3.529	0.832	2.907	0.954
0.169	3.168	12.335	3.496	3.528	0.844	2.952	0.972
0.198	3.216	12.335	3.536	3.489	0.852	3.013	0.980
0.250	3.286	12.335	3.606	3.420	0.862	3.109	0.988
0.300	3.354	12.335	3.667	3.364	0.873	3.200	0.999
0.400	3.431	12.335	3.774	3.268	0.880	3.322	1.002
0.520	3.486	12.335	3.861	3.194	0.884	3.414	1.001
0.660	3.540	12.335	3.952	3.121	0.887	3.507	1.000
0.710	3.566	12.335	3.996	3.087	0.889	3.553	1.000
0.800	3.613	12.335	4.072	3.029	0.892	3.634	1.000
0.900	3.676	12.335	4.174	2.955	0.897	3.743	1.000
1.000	3.737	12.335	4.276	2.885	0.901	3.851	1.000
1.100	3.777	12.335	4.344	2.839	0.903	3.923	1.000
1.200	3.777	12.335	4.344	2.839	0.903	3.923	1.000
1.300	3.777	12.335	4.344	2.839	0.903	3.923	1.000
1.400	3.777	12.335	4.344	2.839	0.903	3.923	1.000
1.500	3.777	12.335	4.344	2.839	0.903	3.923	1.000
1.600	3.737	12.335	4.276	2.885	0.901	3.851	1.000

TABLE IV(a).– SURFACE DATA

20 DEGREE FLARE

S(CM)	PW/PW INF	S(CM)	QW/QW INF
-11.3	0.97	-12.06	0.98
-10.3	0.98	-10.80	1.05
-9.3	0.96	-9.52	1.06
-8.3	0.98	-8.26	1.02
-7.3	0.97	-6.98	1.03
-6.3	0.99	-5.73	1.00
-5.3	1.03	-4.44	1.03
-4.3	1.00	-3.18	1.01
-3.3	1.02	-1.90	0.99
-2.3	1.00	-0.64	0.86
-1.3	1.09	1.1	4.79
1.1	2.02	1.6	4.17
1.6	3.68	2.1	4.99
2.1	5.31	2.6	5.27
2.6	5.96	3.1	5.94
3.6	7.42	3.6	5.74
4.1	8.27	4.6	6.04
4.6	9.10	5.1	7.99
5.1	9.95	6.1	8.59
6.1	10.80	7.1	8.74
7.1	11.30	8.1	8.64
10.1	12.14	9.1	8.77
12.1	12.26	10.1	9.18
14.1	12.50	12.1	9.68
		13.1	9.59
		14.1	9.36
		15.1	8.55

TABLE IV(b).– SURFACE DATA

30 DEGREE FLARE

S(CM)	PW/PW INF	S(CM)	QW/QW INF
-11.3	1.00	-12.06	0.99
-10.3	0.98	-10.80	0.99
-9.3	0.97	-9.52	1.00
-8.3	0.98	-8.26	1.00
-7.3	1.00	-6.98	1.01
-6.3	1.00	-5.73	1.01
-5.3	0.98	-4.44	1.00
-4.3	1.02	-3.18	0.99
-3.3	1.09	-1.90	0.99
-2.3	1.39	-0.64	1.02
-1.3	1.73	1.1	8.20
1.1	7.75	1.6	8.97
1.6	9.58	2.1	10.09
2.1	12.85	3.1	12.05
2.6	15.06	3.6	13.42
3.6	19.51	4.6	14.39
4.1	21.33	5.1	15.25
4.6	21.94	6.1	14.86
6.1	22.82	7.1	14.90
7.1	22.88	8.1	14.60
8.1	23.71	9.1	14.75
10.1	24.40	10.1	14.45
12.1	23.62	11.1	14.41
14.1	22.60	12.1	13.98
		13.1	13.02
		14.1	12.87
		15.1	12.21

TABLE IV(c).– SURFACE DATA

32.5 DEGREE FLARE

S(CM)	PW/PW INF	S(CM)	QW/QW INF
-11.3	1.01	-12.06	1.00
-10.3	0.99	-10.80	0.99
-9.3	0.98	-9.52	1.00
-8.3	1.01	-8.26	1.01
-7.3	0.97	-6.98	1.03
-6.3	1.01	-5.73	1.01
-5.3	1.03	-4.44	1.05
-4.3	1.12	-3.18	1.09
-3.3	1.23	-1.90	1.33
-2.3	1.71	-0.64	2.16
-1.3	2.56	1.05	6.79
0.55	5.85	1.55	7.44
1.05	7.50	2.05	9.23
1.55	8.42	2.55	10.64
2.05	12.02	3.05	12.82
2.55	14.40	3.55	14.55
3.55	21.19	4.55	16.28
4.05	23.57	5.05	17.05
4.55	25.83	6.05	17.05
6.05	27.14	7.05	16.67
7.05	27.74	8.05	16.41
8.05	27.62	9.05	16.54
10.05	27.74	10.05	15.90
		11.05	15.77

TABLE IV(d).– SURFACE DATA

35 DEGREE FLARE

S(CM)	PW/PW INF	S(CM)	QW/QW INF
-11.3	0.97	-12.06	0.99
-10.3	0.98	-10.80	1.07
-9.3	1.00	-9.52	1.00
-8.3	1.15	-8.26	1.04
-7.3	1.45	-6.98	1.02
-6.3	2.01	-5.73	1.26
-5.3	2.53	-4.44	1.83
-4.3	3.25	-3.18	2.39
-3.3	3.63	-1.90	2.63
-2.3	4.41	-0.64	2.55
-1.3	4.56	1.07	6.40
1.07	6.95	1.57	7.90
1.57	8.82	2.07	9.65
2.07	11.07	2.57	11.75
2.57	14.05	3.07	13.82
3.07	18.45	3.57	16.10
3.57	21.79	5.07	20.03
4.07	25.71	6.07	21.96
4.57	28.93	7.07	21.37
7.07	33.68	9.07	19.72
8.07	33.69	10.07	19.97
10.07	30.04		

TABLE VI(a).– SURFACE DATA

10 DEGREE FIN

TAP NO.	PW/PW INF	GAGE NO.	QW/QW INF
2	2.27	2	1.75
3	1.67	4	1.37
4	1.63	5	1.23
5	1.48	6	1.06
6	1.27	7	1.03
7	1.09	10	1.00
8	1.00		
9	0.99		
10	1.00		
13	1.96	11	1.75
14	1.58	12	1.72
15	1.66	13	1.35
16	1.57	14	1.29
17	1.41	15	1.15
18	1.22	16	1.05
19	1.06	17	1.06
20	1.01	18	1.03
21	1.00	19	1.03
22	1.00	20	0.98

TABLE VI(b).– SURFACE DATA

15 DEGREE FIN

TAP NO.	PW/PW INF	GAGE NO.	QW/QW INF
3	3.40	4	1.69
4	1.73	5	1.65
5	1.88	6	1.58
6	1.84	7	1.40
7	1.60	10	1.02
8	1.29		
9	1.05		
10	1.00		
14	2.98	13	2.00
15	1.71	14	1.48
16	1.84	15	1.58
17	1.94	16	1.46
18	1.81	17	1.17
19	1.58	18	1.02
20	1.29	19	1.00
21	1.08	20	0.97
22	1.00		
23	0.99		

PRECEDING PAGE BLANK NOT FILMED

TABLE VI(c).– SURFACE DATA

20 DEGREE FIN

TAP NO.	PW/PW INF	GAGE NO.	QW/QW INF
5	2.05	4	1.67
6	2.00	5	1.86
7	2.16	6	1.79
8	2.06	7	1.86
9	1.74	8	1.63
10	1.33	9	1.30
11	1.05	10	1.13
16	2.99	14	1.54
17	1.86	15	1.56
18	2.01	16	1.75
19	2.24	17	1.86
20	2.08	18	1.59
21	1.78	19	1.30
22	1.38	20	1.00
23	1.09		

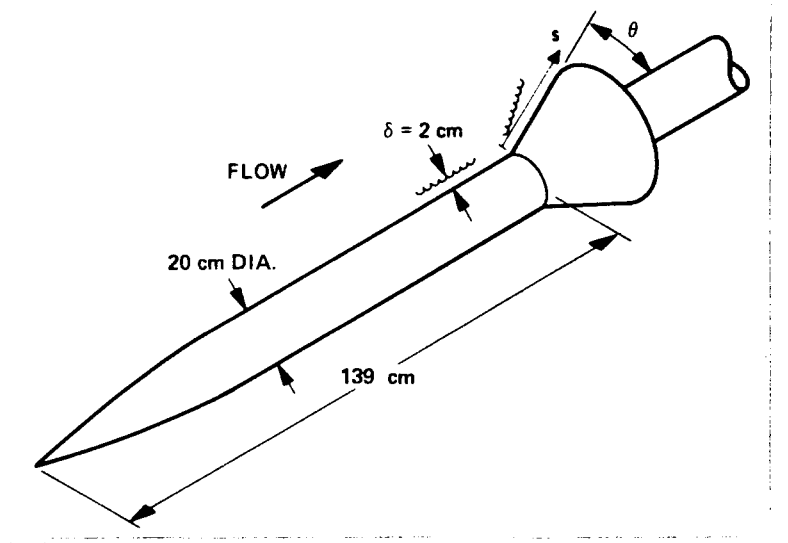

(a)

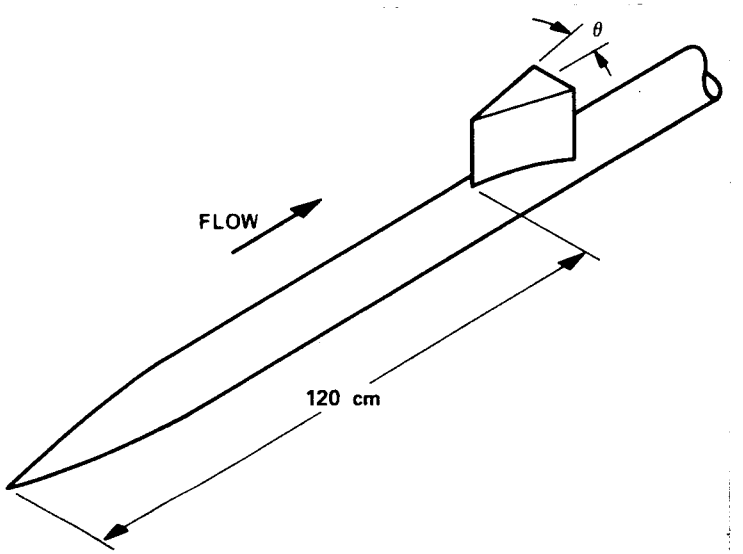

(b)

Figure 1.– Test body. (a) With flare attached. (b) With fin attached.

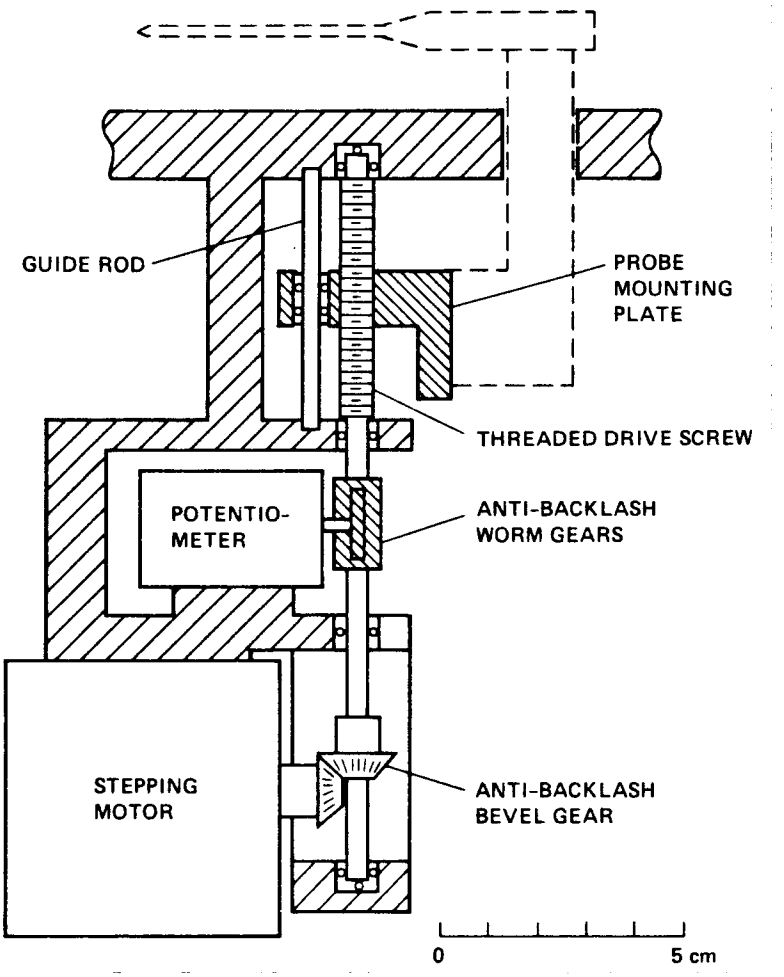

Figure 2.– Survey mechanism.

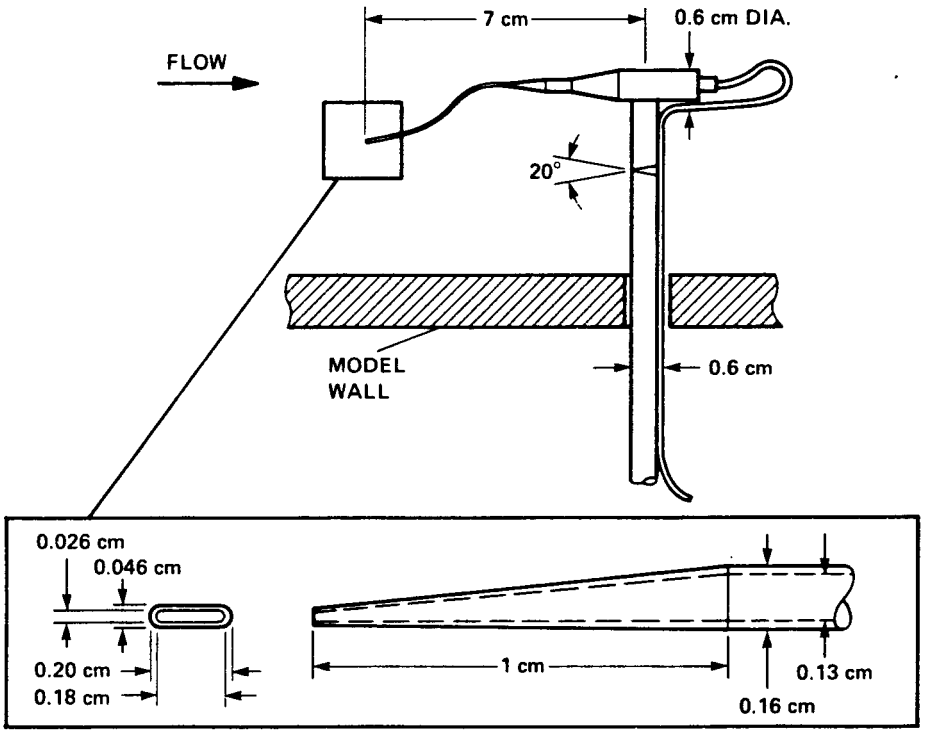

Figure 3.– Pitot pressure probe.

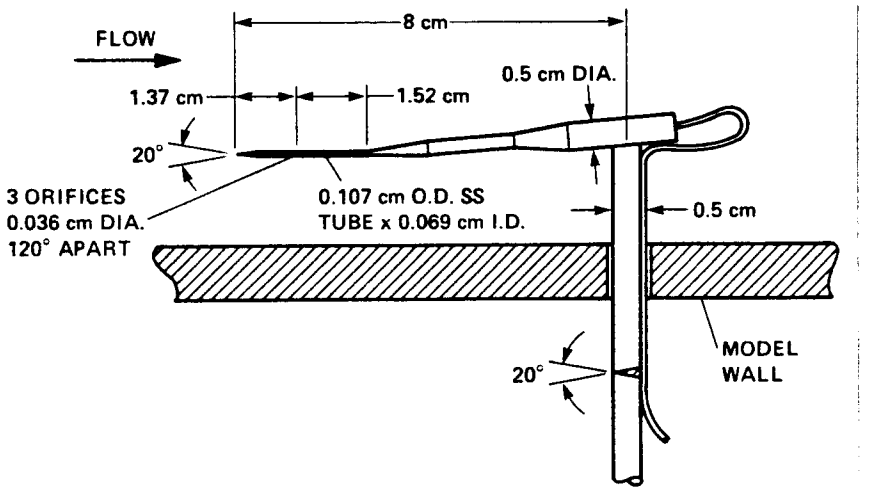

Figure 4.– Static pressure probe.

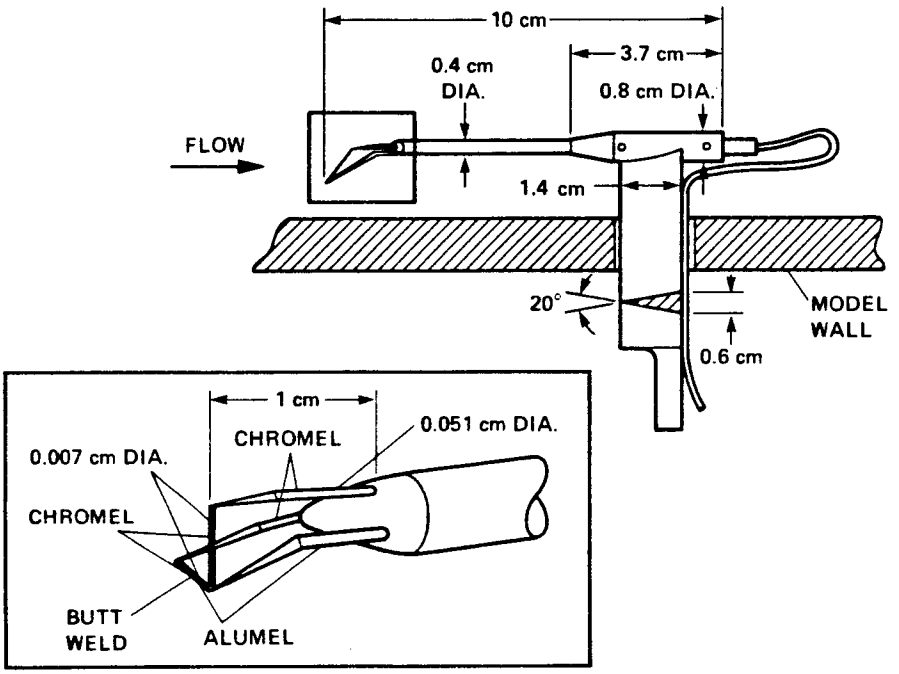

Figure 5.– Total temperature probe.

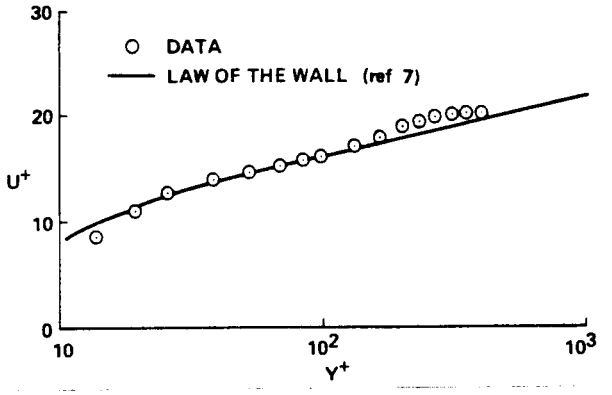

Figure 6.– Mean velocity distributions in law-of-the-wall coordinates for the undisturbed boundary layer.

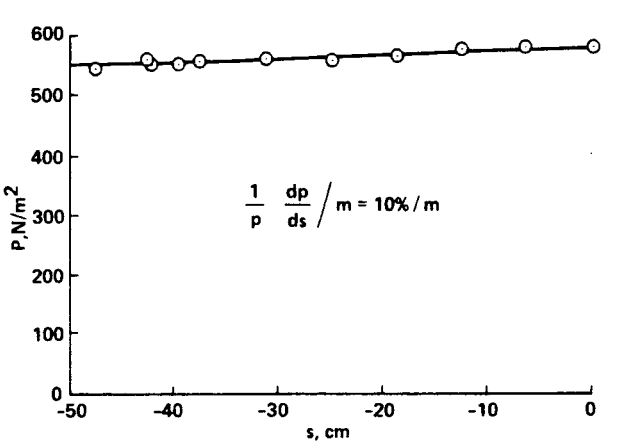

Figure 7.– Surface pressure gradient.

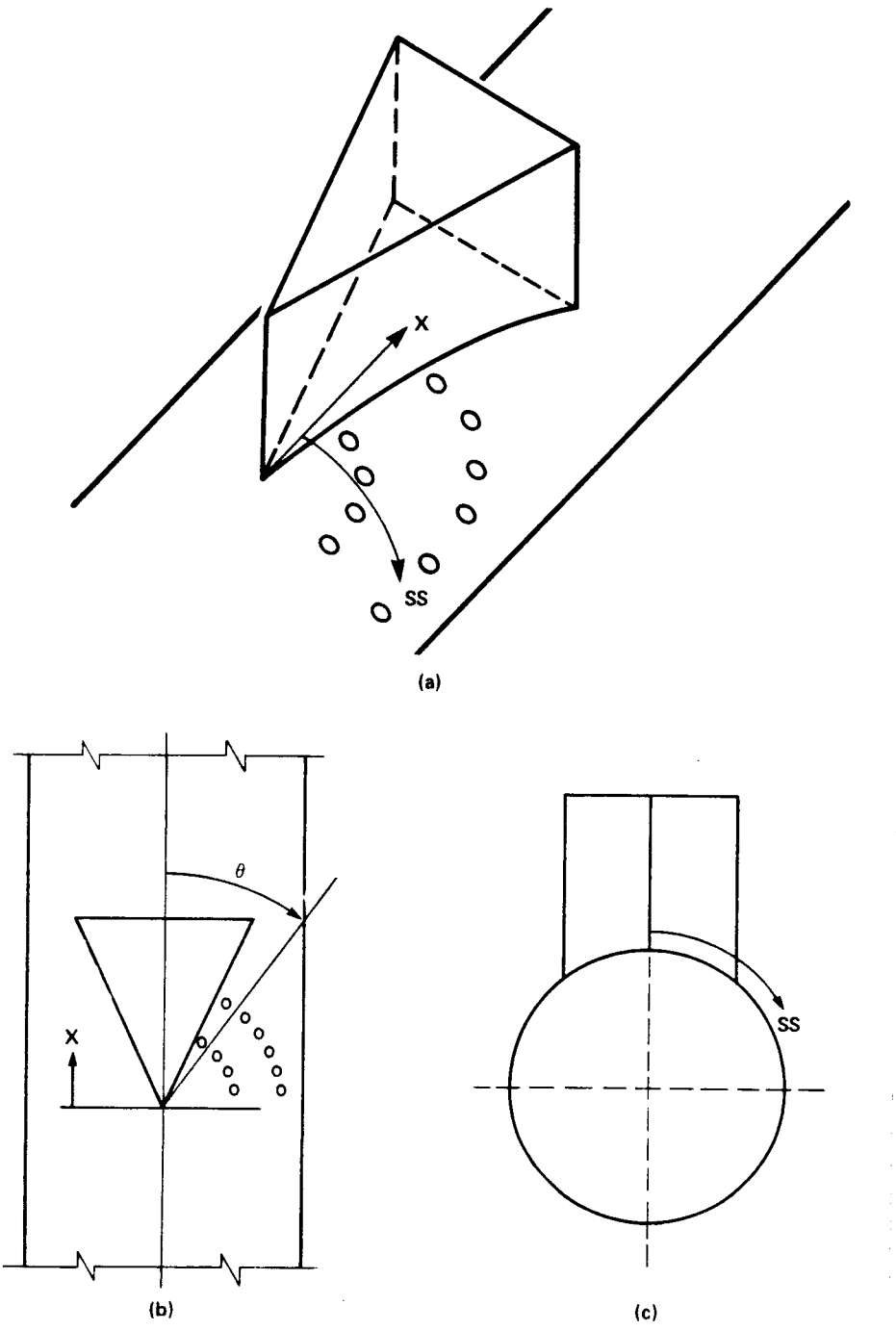

Figure 8.– Location of surface instrumentation locations adjacent to fin.

NASA
National Aeronautics and Space Administration

Report Documentation Page

1. Report No.	2. Government Accession No.	3. Recipient's Catalog No.
NASA TM 101075		

4. Title and Subtitle	5. Report Date
Documentation of Two- and Three-Dimensional Hypersonic Shock Wave/Turbulent Boundary Layer Interaction Flows	6. Performing Organization Code

7. Author(s)	8. Performing Organization Report No.
M. I. Kussoy (Eloret Institute, Sunnyvale, CA) and C. C. Horstman	A-89048
	10. Work Unit No. 505-80-11
9. Performing Organization Name and Address	11. Contract or Grant No.
Ames Research Center Moffett Field, CA 94035	13. Type of Report and Period Covered Technical Memorandum
12. Sponsoring Agency Name and Address	14. Sponsoring Agency Code
National Aeronautics and Space Administration Washington, DC 20546-0001	

15. Supplementary Notes

Point of contact: C. C. Horstman, Ames Research Center, MS 229-1, Moffett Field, CA 94035
(415) 694-5396 or FTS 464-5396

16. Abstract

Experimental data for a series of two- and three-dimensional shock wave/turbulent boundary layer interaction flows at Mach 7 are presented. Test bodies, composed of simple geometric shapes, were designed to generate flows with varying degrees of pressure gradient, boundary-layer separation, and turning angle. The data include surface-pressure and heat-transfer distributions as well as limited mean-flow-field surveys in both the undisturbed and the interaction regimes. The data are presented in a convenient form for use in validating existing or future computational models of these generic hypersonic flows.

17. Key Words (Suggested by Author(s))	18. Distribution Statement
Turbulent boundary layer Hypersonic Shock wave	Unclassified – Unlimited Subject category: 02

19. Security Classif. (of this report)	20. Security Classif. (of this page)	21. No. of pages	22. Price
Unclassified	Unclassified		